Ultrafast optical switching based on nonlinear polarization rotation in silicon waveguides

Jonathan Y. Lee[1], Lianghong Yin[2,3], Govind P. Agrawal[2], and Philippe M. Fauchet[1,2,*]

[1]*Department of Electrical and Computer Engineering, University of Rochester, Rochester, NY, 14627, USA*
[2]*Institute of Optics, University of Rochester, Rochester, NY, 14627, USA*
[3]*Current affiliation: Department of Electrical & Computer Engineering, Rutgers University, Piscataway, NJ, 08854, USA*
**fauchet@ece.rochester.edu*

Abstract: We experimentally realize ultrafast all-optical switching in the 1.5-μm spectral region using cross-phase modulation inside a 5-mm long silicon waveguide. Modulation depths of up to 90% and switching window durations ~1 ps are achieved using 500-fs pump pulses with energies below 10 pJ.

OCIS codes: (190.3270) Kerr effect; (190.7110) Ultrafast nonlinear optics; (230.4110) Modulators; (230.7370) Waveguides; (160.6000) Semiconductor materials.

References and links

1. Q. Lin, O. J. Painter, and G. P. Agrawal, "Nonlinear optical phenomena in silicon waveguides: modeling and applications," Opt. Express **15**(25), 16604–16644 (2007).
2. H. K. Tsang, C. S. Wong, T. K. Liang, I. E. Day, S. W. Roberts, A. Harpin, J. Drake, and M. Asghari, "Optical dispersion, two-photon absorption and self-phase modulation in silicon waveguides at 1.5 μm wavelength," Appl. Phys. Lett. **80**(3), 416–418 (2002).
3. I.-W. Hsieh, X. Chen, J. I. Dadap, N. C. Panoiu, R. M. Osgood, Jr., S. J. McNab, and Y. A. Vlasov, "Cross-phase modulation-induced spectral and temporal effects on co-propagating femtosecond pulses in silicon photonic wires," Opt. Express **15**(3), 1135–1146 (2007).
4. N. Matsuda, R. Shimizu, Y. Mitsumori, H. Kosaka, A. Sato, H. Yokoyama, K. Yamada, T. Watanabe, T. Tsuchizawa, H. Fukuda, S. Itabashi, and K. Edamatsu, "All-optical phase modulations in a silicon wire waveguide at ultralow light levels," Appl. Phys. Lett. **95**(17), 171110 (2009).
5. V. Raghunathan, D. Borlaug, R. R. Rice, and B. Jalali, "Demonstration of a Mid-infrared silicon Raman amplifier," Opt. Express **15**(22), 14355–14362 (2007).
6. H. Fukuda, K. Yamada, T. Shoji, M. Takahashi, T. Tsuchizawa, T. Watanabe, J. Takahashi, and S. Itabashi, "Four-wave mixing in silicon wire waveguides," Opt. Express **13**(12), 4629–4637 (2005).
7. V. R. Almeida, C. A. Barrios, R. R. Panepucci, and M. Lipson, "All-optical control of light on a silicon chip," Nature **431**(7012), 1081–1084 (2004).
8. M. Waldow, T. Plötzing, M. Gottheil, M. Först, J. Bolten, T. Wahlbrink, and H. Kurz, "25ps all-optical switching in oxygen implanted silicon-on-insulator microring resonator," Opt. Express **16**(11), 7693–7702 (2008).
9. T. Tanabe, M. Notomi, S. Mitsugi, A. Shinya, and E. Kuramochi, "All-optical switches on a silicon chip realized using photonic crystal nanocavities," Appl. Phys. Lett. **87**(15), 151112 (2005).
10. D. J. Moss, L. Fu, I. Littler, and B. J. Eggleton, "Ultrafast all-optical modulation via two-photon absorption in silicon-on-insulator waveguides," Electron. Lett. **41**(6), 320–321 (2005).
11. T. K. Liang, L. R. Nunes, T. Sakamoto, K. Sasagawa, T. Kawanishi, M. Tsuchiya, G. R. A. Priem, D. Van Thourhout, P. Dumon, R. Baets, and H. K. Tsang, "Ultrafast all-optical switching by cross-absorption modulation in silicon wire waveguides," Opt. Express **13**(19), 7298–7303 (2005).
12. O. Boyraz, P. Koonath, V. Raghunathan, and B. Jalali, "All optical switching and continuum generation in silicon waveguides," Opt. Express **12**(17), 4094–4102 (2004).
13. M. A. Foster, R. Salem, D. F. Geraghty, A. C. Turner-Foster, M. Lipson, and A. L. Gaeta, "Silicon-chip-based ultrafast optical oscilloscope," Nature **456**(7218), 81–84 (2008).
14. B. G. Lee, A. Biberman, A. C. Turner-Foster, M. A. Foster, M. Lipson, A. L. Gaeta, and K. Bergman, "Demonstration of broadband wavelength conversion at 40 Gb/s in silicon waveguides," IEEE Photon. Technol. Lett. **21**(3), 182–184 (2009).
15. J. Zhang, Q. Lin, G. Piredda, R. W. Boyd, G. P. Agrawal, and P. M. Fauchet, "Optical solitons in a silicon waveguide," Opt. Express **15**(12), 7682–7688 (2007).
16. N. M. Wright, D. J. Thomson, K. L. Litvinenko, W. R. Headley, A. J. Smith, A. P. Knights, J. H. B. Deane, F. Y. Gardes, G. Z. Mashanovich, R. Gwilliam, and G. T. Reed, "Free carrier lifetime modification for silicon waveguide based devices," Opt. Express **16**(24), 19779–19784 (2008).
17. A. C. Turner-Foster, M. A. Foster, J. S. Levy, C. B. Poitras, R. Salem, A. L. Gaeta, and M. Lipson, "Ultrashort free-carrier lifetime in low-loss silicon nanowaveguides," Opt. Express **18**(4), 3582–3591 (2010).

#125253 - $15.00 USD Received 10 Mar 2010; revised 23 Apr 2010; accepted 26 Apr 2010; published 14 May 2010

18. L. Yin, J. Zhang, P. M. Fauchet, and G. P. Agrawal, "Optical switching using nonlinear polarization rotation inside silicon waveguides," Opt. Lett. **34**(4), 476–478 (2009).
19. J. Y. Lee, L. Yin, G. P. Agrawal, and P. M. Fauchet, "Ultrafast Kerr Switching in a Silicon Waveguide," in *Proceedings of 6th international IEEE Conference on Group IV Photonics* (Institute of Electrical and Electronics Engineers, 2009), pp. 95–97.
20. L. Yin, J. Y. Lee, P. M. Fauchet, and G. P. Agrawal, "Realization of an Ultrafast Silicon Kerr Switch," in *Conference on Frontiers in Optics,* (Optical Society of America, 2009), paper FML4.
21. R. H. Stolen, and A. Ashkin, "Optical Kerr effect in glass waveguides," Appl. Phys. Lett. **22**(6), 294–296 (1973).
22. G. P. Agrawal, *Nonlinear Fiber Optics*, 4th ed. (Academic Press, Boston, 2007).
23. S. J. McNab, N. Moll, and Y. A. Vlasov, "Ultra-low loss photonic integrated circuit with membrane-type photonic crystal waveguides," Opt. Express **11**(22), 2927–2939 (2003).
24. D. Dimitropoulos, R. Jhaveri, R. Claps, J. C. S. Woo, and B. Jalali, "Lifetime of photogenerated carriers in silicon-on-insulator rib waveguides," Appl. Phys. Lett. **86**(7), 071115 (2005).
25. Q. Lin, J. Zhang, G. Piredda, R. W. Boyd, P. M. Fauchet, and G. P. Agrawal, "Dispersion of silicon nonlinearities in the near infrared region," Appl. Phys. Lett. **91**(2), 021111 (2007).
26. H. Rong, A. Liu, R. Nicolaescu, M. Paniccia, O. Cohen, and D. Hak, "Raman gain and nonlinear optical absorption measurements in a low-loss silicon wave- guide," Appl. Phys. Lett. **85**(12), 2196–2198 (2004).
27. A. D. Bristow, N. Rotenberg, and H. M. Van Driel, "Two-photon absorption and Kerr coefficients of silicon for 850-2200 nm," Appl. Phys. Lett. **90**(19), 191104 (2007).
28. J. Zhang, Q. Lin, G. Piredda, R. W. Boyd, G. P. Agrawal, and P. M. Fauchet, "Anisotropic nonlinear response of silicon in the near-infrared region," Appl. Phys. Lett. **91**(7), 071113 (2007).
29. L. Yin, and G. P. Agrawal, "Impact of two-photon absorption on self-phase modulation in silicon waveguides," Opt. Lett. **32**(14), 2031–2033 (2007).
30. A. B. Fallahkhair, K. S. Li, and T. E. Murphy, "Vector finite-difference mode solver for anisotropic dielectric waveguides," J. Lightwave Technol. **26**(11), 1423–1431 (2008).
31. H. Rong, R. Jones, A. Liu, O. Cohen, D. Hak, A. Fang, and M. Paniccia, "A continuous-wave Raman silicon laser," Nature **433**(7027), 725–728 (2005).

1. Introduction

Silicon-on-insulator (SOI) is a promising platform for optical interconnects and optical device integration because of its compatibility with the mature CMOS fabrication technology. Recently, silicon has attracted increasing attention for nonlinear applications owing to its strong third-order nonlinearity $\chi^{(3)}$. In addition, the high refractive index of silicon enables tight optical mode confinement, promoting a more effective nonlinear interaction [1]. Therefore, nonlinear optical phenomena in silicon have been extensively studied including self-phase modulation (SPM) [2], cross-phase modulation (XPM) [3,4], stimulated Raman scattering (SRS) [5], and four-wave mixing (FWM) [6]. These interesting nonlinear properties facilitate a variety of applications, such as high-speed all-optical switching [7–12], ultrafast optical oscilloscopes [13], wavelength conversion [14], and soliton formation [15].

Recently, several all-optical switches have been demonstrated. Some are based on the free-carrier plasma effect induced by two-photon absorption (TPA). Silicon microring [7,8] and photonic crystal cavities [9] were demonstrated to modulate continuous-wave probe signal by shifting the resonances due to the free-carrier plasma effect. Even though the lifetime of a free-carrier can be shortened by various methods [8,16,17], it still fundamentally limits the speed of signal modulation. An alternative modulator is based on non-degenerate TPA. A weak probe signal is absorbed through the TPA process when it is co-propagating with an intense pump signal [10,11]. This scheme, however, can only modulate the signal in the form of absorption dips. The third scheme is based on XPM induced by the Kerr effect. One design makes use of a Mach-Zehnder configuration [12]. Such an interferometeric setup enables two conjugated outputs, producing modulated peaks and dips. However, in practice, an interferometer requires intensive phase tuning between its two arms owing to imperfect fabrication, and it has a large footprint.

In this letter, we realize experimentally an ultrafast all optical switch in a 5-mm-long silicon waveguide using XPM-induced nonlinear polarization rotation (NPR), an approach proposed by us recently [18–20]. Such a Kerr shutter has been demonstrated in polarization maintaining optical fibers [21], but until now it has not been realized in silicon waveguides. Our Kerr switch does not require an interferometic configuration, yet we can obtain two modulated signals simultaneously at the output. From the measured bandwidth-limited modulation depth and using the split-step Fourier method [22] to model the results, we

#125253 - $15.00 USD Received 10 Mar 2010; revised 23 Apr 2010; accepted 26 Apr 2010; published 14 May 2010

estimate an original modulation depth ~90% for a pump peak power ~15 W. The autocorrelation traces measured at different pump peak powers agree well with those obtained numerically and show that subpicoseond switching is possible with our scheme. Finally, we suggest several ways to optimize the device performance, which would lead to a low-power and high-speed all-optical modulator.

2. Device fabrication and experimental setup

Waveguides are fabricated on silicon-on-insulator (SOI) wafers with a 3-μm buried oxide layer (BOX) and a thin silicon layer (thickness 400 nm). The waveguides used in our measurements are designed with a width of 600 nm and a height of 400 nm. The fabricated waveguides are air-clad on top and are aligned along the [110] direction on the (100) silicon surface using electron-beam lithography with negative-tone hydrogen silsesquioxane (HSQ) photoresist. Silicon layer is etched by inductively coupled plasma reactive-ion etching (ICP-RIE) with chlorine gas. The inset in Fig. 1 shows the cross section of the fabricated silicon waveguide. In order to reduce coupling losses, we adopt the mode-converter design of Ref. 23. Two mode converters are formed by inversely tapering both ends of the silicon waveguide to a 30-nm-width over a tapering length of 50 μm. Polymer waveguides (width 1.7 μm and height 2.5 μm) are aligned on top of the silicon nano-taper. The polymer waveguides are defined by i-line (365 nm) stepper lithography with misalignment of less than 0.3 μm. The wafers are cleaved along the crystal orientation.

When we couple light into our waveguide through the nano-coupler, high-order modes of the waveguide may be excited. However, their power levels are expected to be much smaller compared to the fundamental mode because of mode mismatching. Moreover, effective mode areas of high-order modes are considerable larger than the fundamental mode. This implies that the nonlinear effects occur mostly for the fundamental mode. In addition, the fundamental mode and high-orders modes do not overlap much inside the waveguide and nonlinear interaction among them is negligible.

To estimate the propagation loss inside our waveguides, we measured the top-scattered light along the waveguide and fitted the intensity decay with an exponential curve, resulting in a loss of 10 ± 2 dB/cm for both the TE and TM modes. Noting that the waveguide supports multiple modes, we actually measure total scattering losses for all modes. High-order modes exhibit higher losses because of a larger overlap of their optical power with rough interfaces. Thus, propagation losses of the two fundamental modes are below 10 dB/cm. Coupling losses are calculated by subtracting propagation losses from the measured insertion loss, resulting in a coupling loss of 7 ± 1 dB for the TE mode and 8 ± 1 dB for the TM mode.

Figure 1 shows our pump-probe experimental setup for the Kerr switch. Pump pulses, generated at 44 MHz from a mode-locked fiber laser, have a full width at half-maximum (FWHM) of 250 fs and are broadened to almost 500 fs before entering the silicon waveguide. This temporal pulse broadening is mainly due to the dispersive and nonlinear effects within different fibers, and we take this into account in our numerical modeling. We access the waveguide with lensed tapered fibers which focus light to a spot diameter of ~2.5 μm. We keep their length to 30 cm (shorter than the nonlinear length of fiber) to avoid any undesired nonlinear effects. In our control experiment, we confirm that this fiber does not exhibit NPR.

#125253 - $15.00 USD Received 10 Mar 2010; revised 23 Apr 2010; accepted 26 Apr 2010; published 14 May 2010

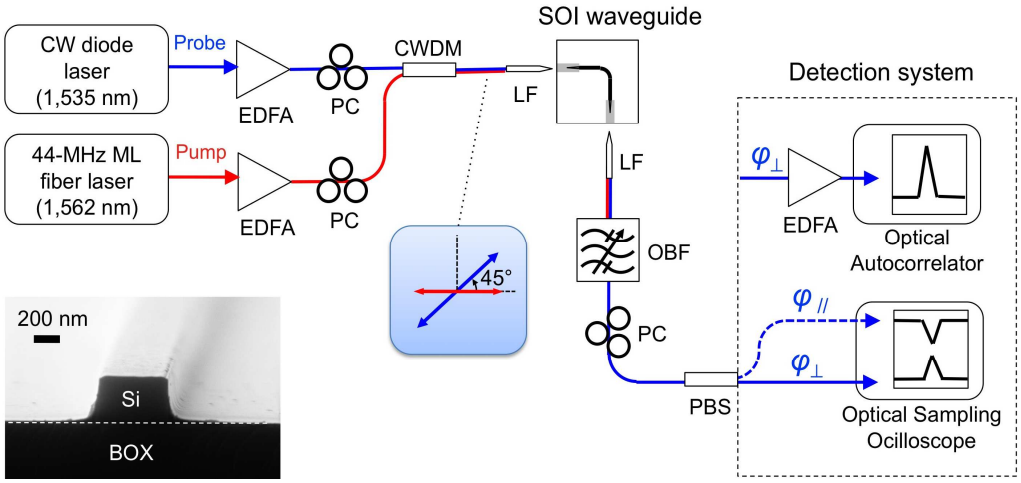

Fig. 1. Experimental setup for the Kerr switch. EDFA, erbium-doped fiber amplifier; PC, polarization controller; CWDM, coarse wavelength-division multiplexer; LF, lensed fiber; OBP, optical bandpass filter; PBS, polarization beam splitter. The blue and red lines represent the probe and pump signals, respectively, guided by a single-mode optical fiber. Inset shows the scanning electron micrograph of our silicon waveguide.

The polarization of the pump and the probe is adjusted by polarization controllers such that pump excites the TE mode of the waveguide and the probe is polarized at 45° with respect to the pump Assuming the same coupling loss at the input and output ends, we estimate the average power of the probe inside the silicon waveguide to be 100 mW. We keep the peak power of the pump below 20 W inside the waveguide. As the probe excites both the TE and TM modes, the CW probe becomes elliptically polarized through XPM and pump-induced NPR. At the output end, we block the pump using a narrowband optical filter that passes only the probe. A polarization controller compensates the linear polarization rotation induced by the waveguide birefringence. A polarization beam splitter, acting as an analyzer, allows us to convert the probe's polarization rotation into amplitude modulation, thus realizing optical Kerr switching. We denote the port that transmits the probe fully in the absence of pump as $\varphi_{//}$ and the port that blocks the probe completely as $\varphi_{\perp}$. The duration of the switching window may exceed the width of pump pulses because of walk-off effects and carrier-induced index changes, but these effects play a minor role at low pump powers [18]. We measure the probe outputs using a bandwidth-limited optical sampling oscilloscope (OSO), and a high-resolution optical autocorrelator.

3. Transient time response

Figure 2, showing the measured oscilloscope traces of the two probe outputs at a pump peak power of ~19 W inside the silicon waveguide, provides a clear evidence for Kerr switching. To prove experimentally that the switching is indeed due to the NPR effects, we changed the polarization state of the launched CW probe and found no Kerr switching when the probe is polarized to excite either the TE or the TM mode of the silicon waveguide. Figure 2(a) corresponds to the probe output at the $\varphi_{//}$ port. We observe a fast switching dip followed with a long exponential decaying tail. As the detection using the OSO is bandwidth-limited, the width of the switching dip is overvalued and the modulation depth is undervalued. Oscillations after the dip are also caused by the limited electrical bandwidth of the detection system. Both XPM and TPA contribute to the fast switching dip. The long tail has its origin in the TPA-induced free-carriers accumulated during the pump pulse and its decay time of 2.4 ns is consistent with the free-carrier lifetime in a silicon waveguide calculated by others [24]. Figure 2(b) shows the probe output signal at the $\varphi_{\perp}$ port. In contrast to what is observed at the $\varphi_{//}$ port, TPA reduces the modulation amplitude. The most noteworthy feature is that the free-

#125253 - $15.00 USD Received 10 Mar 2010; revised 23 Apr 2010; accepted 26 Apr 2010; published 14 May 2010

carrier exponentially decaying tail is absent in this case, which is beneficial for high-speed switching applications.

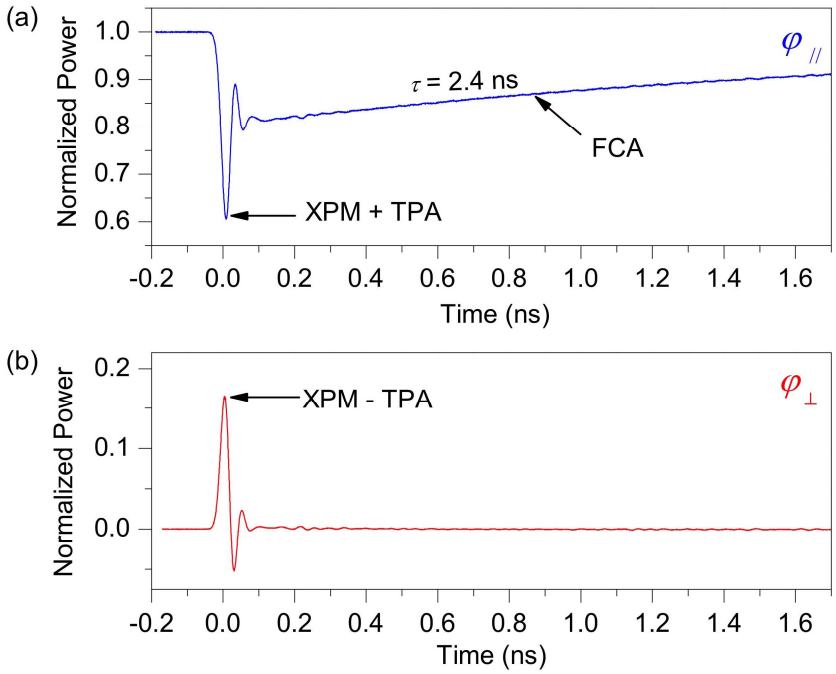

Fig. 2. Measurements of the modulated probe signal using a bandwidth-limited oscilloscope. Temporal responses of the probe at outputs (a) $\varphi_{//}$ and (b) $\varphi\perp$ show clear evidence of Kerr switching. The long tail is not observed at the $\varphi\perp$ port, indicating that it will not limit the repetition rate when this port is employed.

We can estimate the number of free-carrier generated in any distance z by using

$$N_{gen}(z) = \int \frac{\beta_{TPA}}{2h\nu} I^2(z,t)dt, \qquad (1)$$

where $\beta_{TPA} \approx 5 \times 10^{-12}$ m/W [25]. Doing the integral for a sech-pulse shape, we calculate that a single pump pulse generates free carriers with a density of 2.63×10^{23} m^{-3} at the front end of the waveguide, and this density decreases exponentially because of TPA and propagation losses. Using $\alpha_f = \sigma N_{gen}$ with $\sigma = 1.45 \times 10^{-21}$ m^2 [26]. We estimate free-carrier absorption (FCA) to be below 0.88 dB/cm, a value that agrees with the observed amplitude of the long tail.

4. Depth of modulation

4.1 Bandwidth-limited measurement

Figure 3(a) shows how the measured modulation depth, defined as the modulation amplitude divided by the maximum probe transmission at $\varphi_{//}$, increases with pump peak power for both $\varphi_{//}$ and $\varphi\perp$. The modulation depth for $\varphi\perp$ is smaller than that for $\varphi_{//}$ because TPA reduces the modulation amplitude for $\varphi\perp$ but enhances it for $\varphi_{//}$. To understand these results, we perform numerical simulations using the split-step Fourier method [18,22]. By taking into account the 7.3-GHz bandwidth of the detection system, we are able to fit the calculated modulation depth [depicted as solid curves in Fig. 3(a)] to the experimental measurements. The TPA effects can be eliminated by shifting the operating wavelength to beyond 2.2 μm so that the photon energy is less than one half of the silicon bandgap [25,27].

#125253 - $15.00 USD Received 10 Mar 2010; revised 23 Apr 2010; accepted 26 Apr 2010; published 14 May 2010

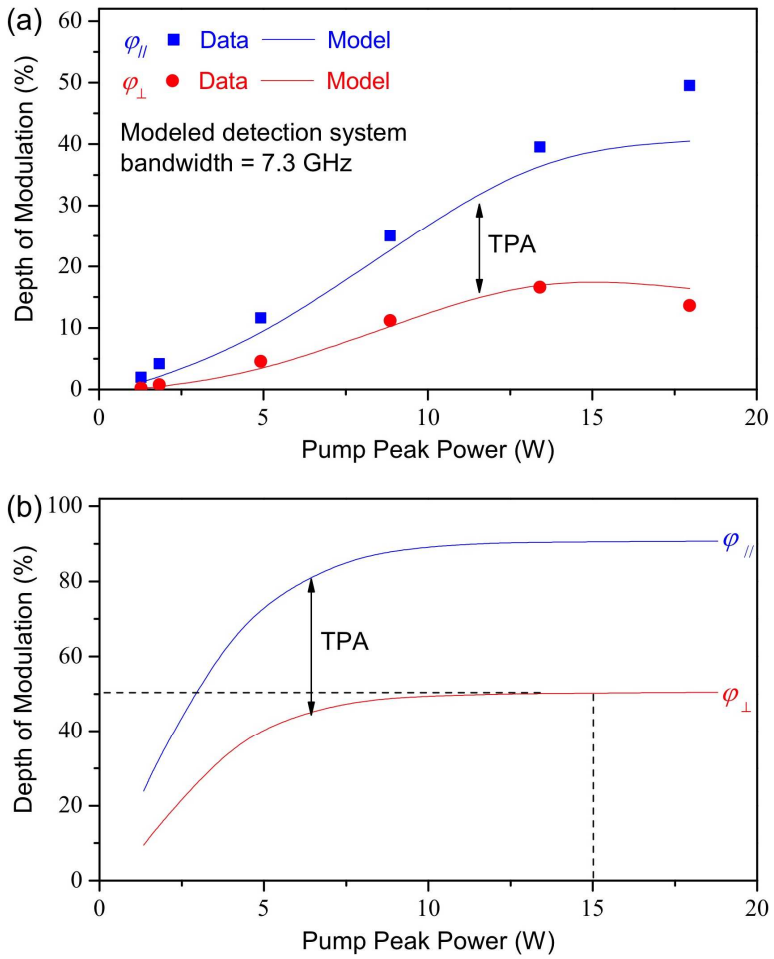

Fig. 3. (a) Measured and calculated modulation depths for the probe outputs at $\varphi_{//}$ and $\varphi_{\perp}$ ports. (b) Simulated modulation depths assuming an infinite bandwidth for the detection system.

4.2 Infinite-bandwidth calculation

The true modulation depth is obtained by removing the limitation set by the detection bandwidth. We model our experimental results by solving the following three coupled equations with the split-step Fourier transform method [18,22]:

$$\frac{\partial E_x}{\partial z} + d_x \frac{\partial E_x}{\partial T} = 2ik_0 n_2 a(1+ir) I_p E_x - \frac{\sigma}{2}(1+i\mu) N_c E_x - \frac{\alpha_l}{2} E_x + i(\beta_x - \bar{\beta}) E_x, \quad (2)$$

$$\frac{\partial E_y}{\partial z} + d_y \frac{\partial E_y}{\partial T} = 2ik_0 n_2 b(1+ir) I_p E_y - \frac{\sigma}{2}(1+i\mu) N_c E_y - \frac{\alpha_l}{2} E_y + i(\beta_y - \bar{\beta}) E_y, \quad (3)$$

$$\frac{\partial I_p}{\partial z} = -\beta_{TPA} I_p^{\,2} - \sigma N_c I_p - \alpha_l I_p, \quad (4)$$

where E_x and E_y are the probe amplitudes and $I_p = |E_p|^2$ is the pump intensity. We use the following rate equation for the carrier density $N_c(z, T)$:

#125253 - $15.00 USD Received 10 Mar 2010; revised 23 Apr 2010; accepted 26 Apr 2010; published 14 May 2010

$$\frac{\partial N_c}{\partial T} = \frac{\beta_{TPA}}{2h\nu_p} I_p^{\,2}(z,T) - \frac{N_c}{\tau_c}, \tag{5}$$

where $h\nu_p$ is the energy of a pump photon and τ_c is the carrier lifetime. The nonlinear phase shift difference is defined as $\Delta\phi = \phi_x - \phi_y$, where ϕ_x is the phase shift induced on the probe in the TE mode, and the ϕ_y is the phase shift induced on the probe in the TM mode. The CW probe is assumed to be so weak that it does not induce any nonlinear effects. The coefficients a and b indicate that the strength of XPM depends on relative polarizations of the pump and probe. In the case of silicon, $a = (1 + \rho) / 2$ and $b = \rho / 3$, with the anisotropy factor $\rho \approx 1.27$ [28]. The TPA of the pump is governed by $r = \beta_{TPA} / (2\, k_0\, n_2)$, where the Kerr parameter $n_2 = 2.5 \times 10^{-18}$ m^2/W [28] for silicon at wavelengths near 1.5 μm. The other parameters are chosen to be: $\mu = 7.6$ [29], $\tau_c = 2.4$ ns [measured from Fig. 2(a)], and effective mode area $a_{eff} = 0.1$ μm^2. We use $\alpha_l = 5$ dB/cm as it provides the best fit to the experimental data in Fig. 3(a). The hyperbolic secant input pump pulse has a FWHM of 500 fs. Walk-off effects governed by d_x and d_y depend on the wavelength difference between the pump and probe and on the waveguide's linear birefringence. Modal indices are calculated by using the two-dimensional full-vector finite difference mode solver [30].

We show in Fig. 3(b) the results of numerical simulations assuming an infinite bandwidth of detection. We observe that the modulation depth saturates near 90% and 50% for $\varphi_{//}$ and $\varphi\perp$ respectively. The minimum pump peak power required for maximum modulation depth can be calculated by using the nonlinear phase shift difference $\Delta\phi = \pi$. We find that for our waveguide length $\Delta\phi$ reaches π when pump peak power is about 15 W (8.5 pJ per pulse).

5. Switching window

The temporal width of the switching window observed in our experiment is resolved using an autocorrelator. As the power of the probe output is not strong enough to generate a measurable second harmonic signal, we amplify the switched probe signal from the $\varphi\perp$ port with an EDFA. Figure 4(a) shows the normalized, background-free, intensity autocorrelation traces of the probe output at several pump peak powers. For peak powers below 2 W, the FWHM of the traces is 1.1 ps. Assuming a hyperbolic secant shape for the switched probe signal, we estimate the width of the switching window to be 700 fs. The switching window is broader than the pump pulse by 200 fs mainly due to group-velocity mismatch and polarization-mode dispersion. When the pump peak power increases to beyond 2 W, we observe two wide shoulders indicating that the probe shape is strongly distorted and eventually the width of the autocorrelation trace saturates at 8 ps.

Figure 4(b) shows that the autocorrelation traces simulated under experimental conditions agree well with the experimental measurements. At low pump peak powers, the width of the autocorrelation trace is 1 ps. As the pump peak power increases, two shoulders appear and they broaden the width of the autocorrelation trace to near 8 ps. The switching window is broadened due to the strong free-carrier dispersion induced by a combination of the free-carrier and walk-off effects [18]. To optimize the switching window, one can design a square-shape waveguide that minimizes the walk-off effects. By reducing the linear birefringence, the difference between the nonlinear phase shifts imposed on the TE and TM components of the probe is minimized, and a narrow switching window is realized.

#125253 - $15.00 USD Received 10 Mar 2010; revised 23 Apr 2010; accepted 26 Apr 2010; published 14 May 2010

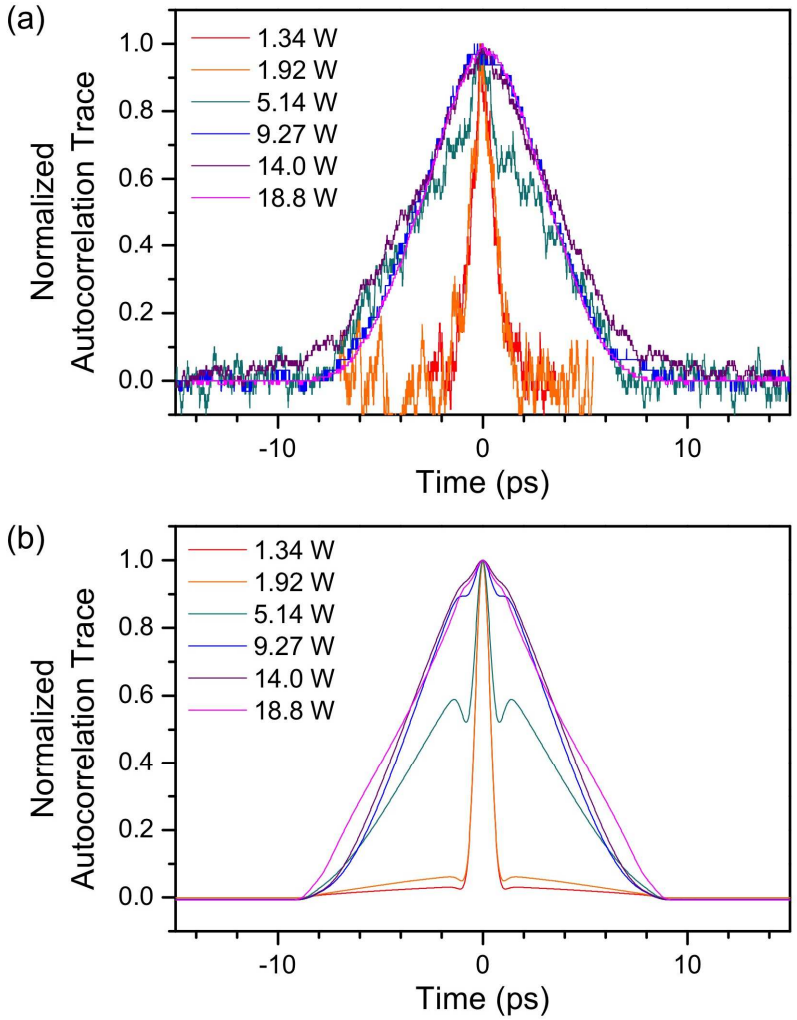

Fig. 4. Switching windows of the modulated probe signal $\varphi\perp$ for different pump peak powers. (a) Measured autocorrelated traces and (b) corresponding numerical simulations.

6. Device optimization

6.1 Minimizing walk-off effects

There are two sources of the walk-off effects: one is the modal dispersion mismatch between the TE and the TM probe signals, and another one is the wavelength separation between the probe and the pump signals. Modal dispersion can be eliminated by designing a symmetric silicon waveguide with a square cross-section. The group velocity mismatch between the pump and probe can be reduced by shifting the zero dispersion between their wavelengths. Figure 5(a) shows the calculated group velocity dispersion (GVD) parameter D of the fundamental mode for different waveguide widths/heights. The group indices are calculated using the two-dimensional full-vector finite difference mode solver [30]. The square shape silicon waveguide is fully buried in oxide. The GVD is zero near 1.55 μm when the silicon waveguide width and height are ~800 nm. However, such a large waveguide cross section will result in a large effective mode area and a reduced effective nonlinearity. This issue may require the use of higher index contrast materials.

#125253 - $15.00 USD Received 10 Mar 2010; revised 23 Apr 2010; accepted 26 Apr 2010; published 14 May 2010

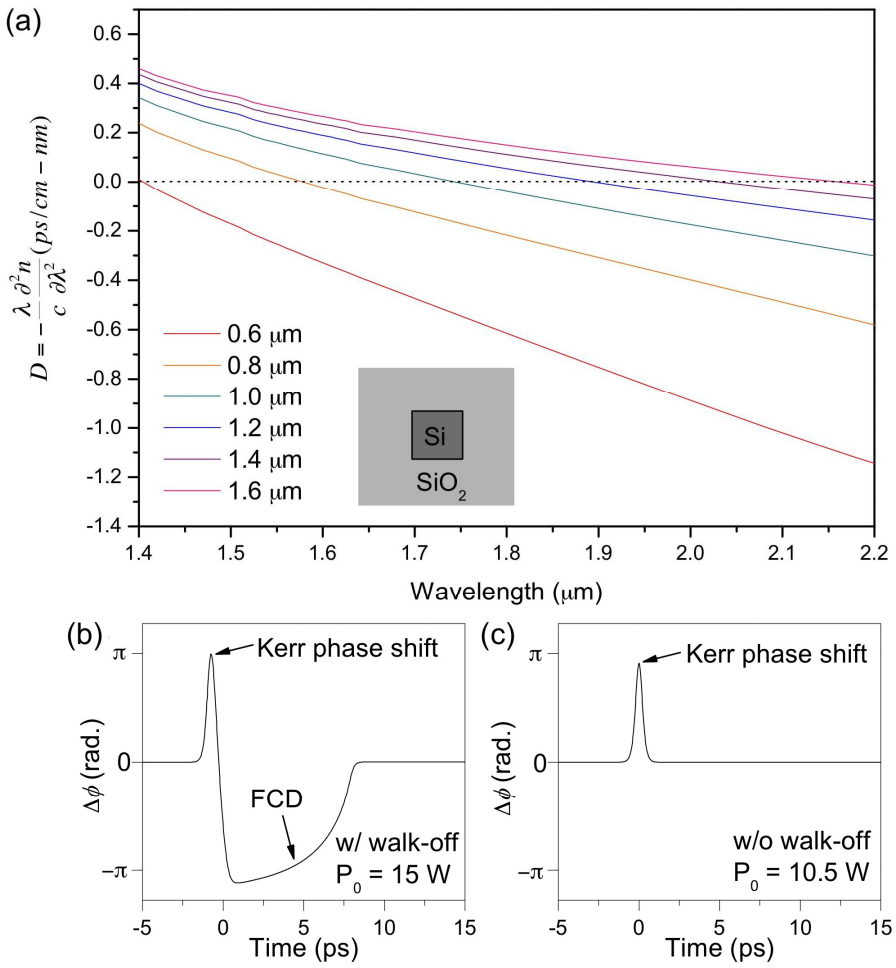

Fig. 5. (a) Calculated dispersion parameters for the fundamental mode in silicon waveguide of different sizes. (b) Calculated nonlinear phase shift difference $\Delta\phi$ induced on the probe signal by a 500-fs pump pulse when its peak power P_0 is at 15 W. (c) Calculated $\Delta\phi$ in the absence of the walk-off effects for a symmetric silicon waveguide with zero dispersion near 1,550 nm.

Figure 5(b) shows the calculated $\Delta\phi$ induced on the probe signal in our model with a strong walk-off. First, $\Delta\phi$ is positive because it is induced by the Kerr effect, then it becomes negative because of free-carrier dispersion induced by TPA. The required pump power to achieve $\Delta\phi = \pi$ can be reduced to near 10.5 W (6 pJ per pulse) if the walk-off effects are minimized by employing a waveguide geometry design shown in Fig. 5(a). The zero-dispersion wavelength can also be shifted toward 1.55 μm to minimize walk off between the pump and probe. In Fig. 5(c), free-carrier dispersion is not observed because the free-carrier phase shift is calculated for the TE and TM modes that are propagating at the same velocity

6.2 Optimizing switching amplitude and switching energy

By minimizing the walk-off effects and the TPA as shown, we can minimize the required switching energy and maximize the switching amplitude. The dotted lines in Fig. 6 represent the experimental situation with walk-off parameters $d_x = -1.6$ ps/cm and $d_y = 16$ ps/cm and TPA coefficient $\beta_{TPA} \approx 5 \times 10^{-12}$ m/W. The required switching energy for achieving a nonlinear phase shift difference $\Delta\phi = \pi$ is 8.5 pJ. By canceling the walk-off, the required

#125253 - $15.00 USD Received 10 Mar 2010; revised 23 Apr 2010; accepted 26 Apr 2010; published 14 May 2010

energy can be reduced to near 6 pJ. However, the maximum switching contrast of the probe at the output $\varphi\perp$ is decreased from 50% to 26%. At the same time, the switching contrast for $\varphi_{//}$ is increased from 91% to ~98%. The larger deviation in switching contrasts between the $\varphi\perp$ and $\varphi_{//}$ outputs suggests stronger TPA effects. If we shift the operating wavelengths to beyond 2.2 μm so that TPA is eliminated, the switching contrast can be up to 100% for both $\varphi\perp$ and $\varphi_{//}$, as predicted from energy conservation. Note that for the output $\varphi\perp$, the switching contrast is improved by almost 4 times.

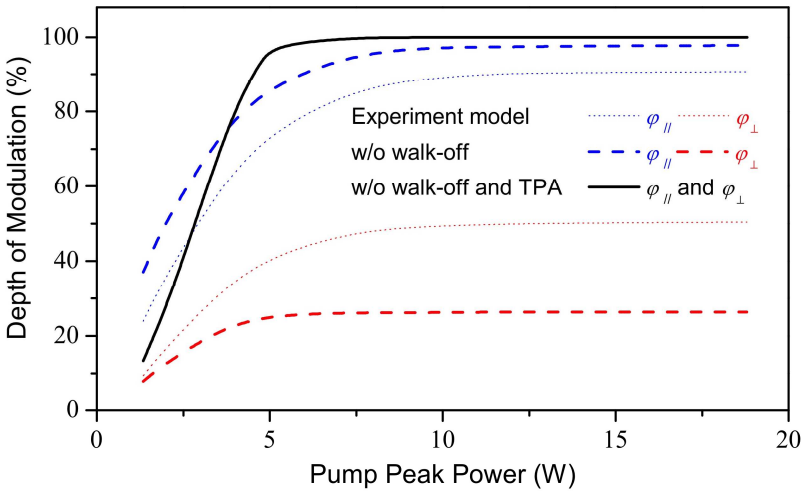

Fig. 6. Comparison of calculated modulation depths as a function of pump peak power for different cases of optimization. The dotted lines correspond to the experiment. The dashed lines are obtained by including TPA but neglecting walk-off. The black line is the ideal case without TPA and walk-off effects.

7. Conclusions

We have successfully realized NPR-induced Kerr switching using SOI waveguides and measured a switching window as narrow as 700 fs for the modulated signal at the $\varphi\perp$ port. The modulation depth can be increased to close to 100% if we minimize TPA by shifting the operation wavelength to beyond 2.2 μm. The walk-off effects limit the ultimate duration of the switching window, but it can be minimized by designing the waveguide properly. By reducing the free-carrier lifetime and using ultrashort pump pulses, it should be possible to reduce the density of free carriers, which will improve the modulation speed. By applying a reverse bias voltage to sweep out the free carriers [17,31], or implanting ions in the silicon to increase free-carrier recombination rates [8,16], it may be possible to operate the switch at repetition rates well beyond 10 Gb/s. With these improvements, we believe that this device can become a practical platform for ultrafast, low-power, all-optical switching and modulation.

Acknowledgments

This work was supported in part by the National Science Foundation (NSF) award ECCS-0801772. Fabrication was performed in the Cornell Nano-Scale Science and Technology Facility (CNF). We acknowledge Jidong Zhang for helping us with the initial waveguide fabrication, and Brian Daniel for helpful discussion.[

#125253 - $15.00 USD Received 10 Mar 2010; revised 23 Apr 2010; accepted 26 Apr 2010; published 14 May 2010